van der Waals Corrected Density Functionals for Cylindrical Surfaces: Ammonia and Nitrogen Dioxide Adsorbed on a Single-Walled Carbon Nanotube

Shah Tanvir ur Rahman Chowdhury[1*], Hong Tang[1†], and John P. Perdew[1,2‡]

[1]*Department of Physics, Temple University, Philadelphia, Pennsylvania 19122, USA,*
[2]*Department of Chemistry, Temple University, Philadelphia, Pennsylvania 19122, USA*

Abstract

We extend the damped Zaremba-Kohn model (dZK) for long-range dispersion interaction between a molecule and a planar surface [J. Tao, H. Tang, A. Patra, P. Bhattarai, and J. P. Perdew, Phys. Rev. B 97, 165403 (2018)] to molecules adsorbed on a curved cylindrical surface, and employ this extended model as an additive correction to the semilocal density functionals PBE and SCAN. The resulting PBE-vdW-dZK and SCAN-vdW-dZK are applied to two systems, NH_3 and NO_2 molecules adsorbed on a single-wall carbon nanotube (CNT), for calculations of binding energies and equilibrium distances. For comparison, the results from vdW nonlocal functionals, such as SCAN+rVV10 and PBE+rVV10, are also presented. The binding energies from PBE+rVV10, SCAN+rVV10, PBE-vdW-dZK, and SCAN-vdW-dZK are about 70-115meV for the system of CNT+NH_3 and 300-500meV for the system of CNT+NO_2. The results from PBE-vdW-dZK and SCAN-vdW-dZK are closer to each other than those from PBE+rVV10 and SCAN+rVV10 are. The relatively closer results from PBE-vdW-dZK and SCAN-vdW-dZK indicate the consistency of our developed vdW-dZK model for cylindrical surfaces. All methods, including PBE, SCAN, PBE+rVV10, SCAN+rVV10, PBE-vdW-dZK, and SCAN-vdW-dZK, give approximately the same binding energy differences between two adsorption configurations (types I and II) for the two systems. This implies that the two adsorption sites have approximately the same adsorption stability. The exponent of the vdW interaction power law from our vdW-dZK model for the two systems is about 0 at short distance, largely due to the damping factor, and tends slowly to $-4 \sim -4.5$ at distances D about 20-50 Å. This feature is very similar to the one calculated with random-phase approximation and renormalization group approaches, supporting the applicability of our methods. Our developed vdw-dZK method provides a highly efficient and reliable method for large systems with cylindrical surfaces, such as vdW interactions with nanotubes.

INTRODUCTION

van der Waals (vdW) interactions are considered to be only a small contribution to the total energy [1, 2]. However, they are a key factor in describing the binding properties in a majority of molecular systems and materials. Although vdW interaction generally includes all intermolecular interactions, it more specifically (and everywhere here) refers to the London dispersion interaction [3,4], a universal interaction between any pair of objects made of electrons. vdW interactions are strongly nonlocal, extending to distances exceeding 10 nm (or 100 Å) in nanoscale materials [5]. London-dispersion-based vdW interaction can be negligible in most solid systems; however, it has non-negligible effects in alkali metals [6], and plays a significant role in molecular complexes, molecular crystals, layered materials, surface adsorptions, and many biosystems. Its influence ranges from drug binding in proteins and double-helix stability in DNA [7] to pedal adhesion in geckos [8,9] and cohesion in asteroids [10,11]. While the importance of understanding and modeling vdW interactions in realistic systems can hardly be overemphasized, our ability to accurately model vdW interactions from first principles is severely

* Email address: tanvir.chowdhury@temple.edu
† Corresponding author, email address: hongtang@temple.edu
‡ Email address: perdew@temple.edu

impeded by the high computational cost of the high-level methods. The adiabatic connection fluctuation-dissipation (ACFD) theorem [12,13], or (after simplifying the interacting density response function) the random phase approximation (RPA) [14,15], plays a central role in understanding the exact treatment of vdW interactions. However, the literature clearly lends support to the view that the ACFD or RPA based methods are not computationally efficient for large systems with over several hundreds of atoms per supercell. Therefore, many more efficient approaches (DFT-vdW) have been developed within the framework of density functional theory (DFT), as long-range additive corrections to semilocal approximations to the density functional for the exchange-correlation energy. These include the vdW-DF family [16-22], VV10 (Vydrov and Van Voorhis) [23] and rVV10 [24], DFT+D series [25, 26], and Tkatchenko-Scheffler (TS) methods [27-29]. These broadly support the view that DFT-vdW combined methods are perhaps one of the most efficient ways to include vdW interactions.

Carbon is a remarkable element showing a variety of stable forms [30] ranging from 3D semiconducting diamond to 2D semimetallic graphite to 1D conducting and semiconducting carbon nanotubes to 0D fullerenes, which show many interesting properties. Single-walled carbon nanotubes [31] (CNTs) are promising materials and building blocks for future nanoelectronics [32-34], due to their large surface area to volume ratios, unique electronic properties, as well as high chemical and mechanical stabilities.

Kong et al. [35] established a connection between the electrical conductivity of single-walled CNTs and their exposure to gaseous molecules such as NO_2 and NH_3. Inspired by their work, Chang et. al. [36] carried out a detailed study of the adsorption of NH_3 and NO_2 on CNTs. They emphasized designing the geometry and computing the binding energy, equilibrium distances, and charge transfers. However, they only took the local density functional (LDA) [37] into consideration and implemented double-numerical basis functions (DND) to compute the binding energies and equilibrium distances. Unfortunately, LDA does not correctly capture the medium and long-range interactions, and therefore the functional approximations needed to be modified. This realization motivated us to investigate the binding energies and equilibrium distances using GGA and meta-GGA functionals, i.e., Perdew-Burke-Ernzerhof (PBE) [38] and the strongly constrained and appropriately normed (SCAN) meta-generalized gradient approximation (meta-GGA) [39].

A natural question arises regarding the vdW interaction relating to nanotubes: to what extent does the vdW energy expression change from a flat to a cylindrical surface? Emig *et al*. [40], starting from the path integral representation, derived the exact Casimir force between a plate and a cylinder. They found the force has an unexpectedly weak decay at large plate-cylinder separations, due to transverse magnetic modes. Rajter *et al*. [41] derived the formulas of vdW interactions for plate-cylinder, cylinder-cylinder systems, based on the Lifshitz theory. Starting from the vdW interaction between two separated semi-infinite half spaces, they then treated the half space as a composite of cylinder bundles and derived the vdW interactions for plate-cylinder and cylinder-cylinder systems. Their formulas can apply to systems made of metallic, semiconducting, and dielectrically isotropic or anisotropic materials, such as semiconducting or metallic carbon nanotubes. In general, vdW interactions are remarkably sensitive to the geometry and electronic structure of a given system. In this work, by using classical electrostatics starting from a dipole outside a cylindrical surface, we put forth a derivation of an expression for vdW

energy between a particle and a cylinder. The particle-cylinder system is a prototype for molecules adsorbed to nanotubes. By using the developed formula, we compute the binding energies and equilibrium distances using our vdW model for NO_2 and NH_3 molecules adsorbed on CNTs. The present work is an extension of our developed damped Zaremba-Kohn model (vdW-dZK) model, which starts from a formula for the vdW interaction of a distant atom with a planar solid surface [42], both with known properties, damps this formula at short range, and then treats an adsorbed molecule or atomic layer as a collection of renormalized atoms. The vdW-dZK model has previously been successfully applied to study the physisorption of graphene and thiophene on metals [43-45] and graphene adsorbed on layered materials [46]. We also compare our results with GGA and meta-GGA combined with rVV10 [23, 24]. In the present work as in other DFT-vdW approaches, the semilocal density functional provides the short- to intermediate range interactions, while the fully nonlocal vdW term provides the intermediate- to long-range interactions, each term doing what it can do best.

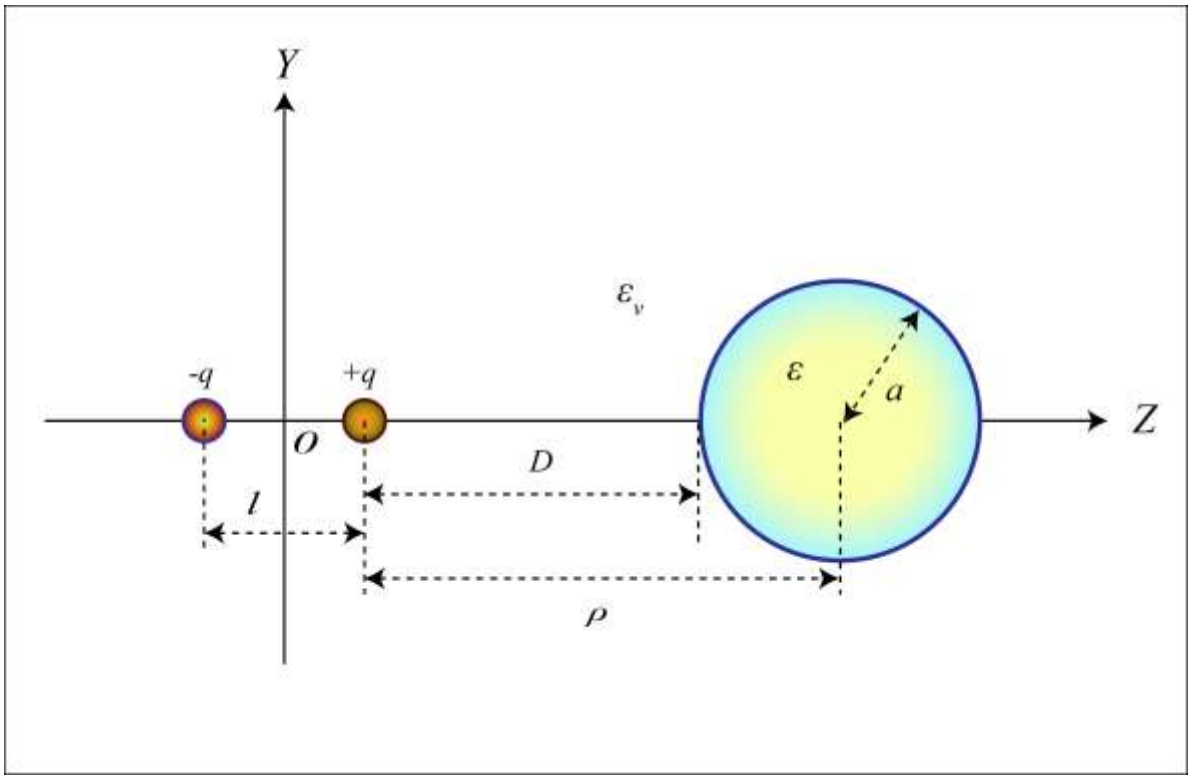

FIG. 1. Schematic diagram of an interacting system consisting of a dipole and a dielectric cylinder. The origin of the coordinate system is at the center of the dipole. The cylinder has a relative dielectric constant ε and a radius a. The relative dielectric constant of the surrounding vacuum is $\varepsilon_v = 1$.

THEORETICAL METHODS

The adsorbed molecules we study here have permanent dipole moments that interact with the static charge densities they induce in the carbon nanotube substrate. That effect is already correctly included via the Hartree electrostatic energy in the approximate density functional calculations we present here. But time-dependent fluctuations of the electron densities around their static averages give

rise to fluctuating dipole moments whose interaction creates the long-range dispersion attraction that is missing from semilocal approximations to the density functional for the exchange-correlation energy. Just as the Zaremba-Kohn treatment of the dispersion interaction starts from the interaction of a static dipole with a planar surface, we will start here from the interaction of a static dipole with a curved cylindrical surface. (The planar surface will emerge as the infinite-radius limit of the cylindrical surface, to make contact with Zaremba-Kohn theory.)

We start by calculating a dipole moment p, $p = ql$, in front of a dielectric cylinder with a radius a. The distance from the positive charge to the surface of the cylinder is denoted D. Consequently, ρ is defined as $D + a$. The direction of the dipole is perpendicular to the longitudinal central axis of the cylinder and pointed towards the cylinder. The origin of the coordinate system is at the center of the dipole, as shown in Fig. 1. Note that the dipole moment p here should be understood as an instantaneous dipole moment, not a permanent one. This means that p (hence q and l) is time dependent. The average of this dipole moment over a long period of time should be zero. However, the time average of p^2 (or $q^2 l^2$) is not zero and will give the dispersion interaction. Since the vdW interaction is the interaction between fluctuating dipoles (or multipoles) at the electrostatic limit, we start from calculating the electrostatic interaction energy between a static dipole and the cylindrical surface.

The electrostatic interaction energy, E_{dipole}^{static}, between the dipole moment $p = ql$ and the charge density it induces in the dielectric cylinder can be calculated as a sum of two parts E_1 and E_2, where the first part E_1 corresponds to the total electrostatic potential energy of the positive charge in the dipole moment p interacting with all the image charges residing inside the cylinder, and similarly, the second part E_2 corresponds to that of the negative charge in the dipole moment p interacting with all the image charges inside the cylinder.

The electric potential at a position $\vec{r}$, produced solely by a point charge q located at a position $\vec{r}'$ outside of a cylinder, is given by the following Green's function,

$$G_0(\vec{r}, \vec{r}') = \frac{q}{\varepsilon_v |\vec{r} - \vec{r}'|}, \tag{1}$$

where ε_v is the relative dielectric constant of the vacuum surrounding the cylinder ($\varepsilon_v = 1$). All units are in atomic units unless otherwise specified. Eq. (1) can be expanded in cylindrical coordinates (ρ, z, ϕ), where the z axis is the central axis of the cylinder [47, 48], as

$$G_0(\vec{r}, \vec{r}') = \frac{4q}{\pi \varepsilon_v} \int_0^\infty dk \, cosk(z - z') \left[\frac{1}{2} I_0(k\rho_<) K_0(k\rho_>) + \sum_{m=1}^{\infty} I_m(k\rho_<) K_m(k\rho_>) \cos m(\phi - \phi') \right], \tag{2}$$

where I_m and K_m are the modified Bessel functions of m-th order. These functions are defined, and their limits at small and large argument are presented, in Ref. [48]. $\rho_<$ or $\rho_>$ indicates the smaller or larger radial coordinate of the source and field points. k denotes a variable in the integration. ϕ and ϕ' are the

azimuth angles relating to the field and source points, respectively. z and z' are the z-coordinates of the field and source points, respectively. Using the above result and applying boundary conditions, the general form of the electric potential *outside* the cylinder, produced *only* by the image charges residing inside the cylindrical medium, is given by (see Eq. (30) of Ref. [48]),

$$G(\vec{r},\vec{r}') = \frac{-2}{\pi\varepsilon_v}\int_0^{\infty} dk\, cos\, k(z-z')\left[\sum_{m=-\infty}^{+\infty} q_m(k)\frac{I_m(ka)}{K_m(ka)}K_m(k\rho_<)K_m(k\rho_>)\, cos\, m(\phi-\phi')\right]. \quad (3)$$

Here a charge q at position $\overrightarrow{r'}$ outside the cylinder produces image charges inside the cylinder which in turn create a potential at $\vec{r}$ outside the cylinder. In Eq. (3), $q_m(k)$ is a constant to satisfy the boundary conditions. It is expressed as

$$q_m(k) = \frac{q(\varepsilon-\varepsilon_v)}{\varepsilon-\varepsilon_v\, h_m(k)}, \qquad m = 0, \pm1, \pm2, \dots, \pm\infty, \quad (4)$$

with

$$h_m(k) = \frac{I_m(ka)K'_m(ka)}{I'_m(ka)K_m(ka)}, \quad (5)$$

where ε is the relative dielectric constant of the cylinder. From Eq. (2) to Eq. (3), the symmetry properties of the modified Bessel function (i.e., $I_{-m}(x) = I_m(x)$ and $K_{-m}(x) = K_m(x)$) are used. Please note that Eqs. (2) and (3) are expressed in a cylindrical coordinate system as in Ref. 48. This is different from the coordinate system in figure 1. However, $\rho_<$ or $\rho_>$ in Eqs. (2) and (3) is related to ρ (ρ_+ or ρ_-) in figure 1. ρ_+ is the distance between the positive charge and the central axis of the cylinder and $\rho_+ = \rho = D + a$, and similarly, ρ_- is the distance between the negative charge and the central axis of the cylinder and $\rho_- = \rho + l = D + a + l$, as can be seen in figure 1. We will use Eq. (3) to calculate E_{dipole}^{static}, which includes E_1 and E_2. In figure 1, since the source or field point is either the positive or the negative charge, and the source and field points are on the same line perpendicular to the central axis of the cylinder, it follows that, in Eq. (3), we have $z = z'$ and $\phi = \phi'$, and Eq. (3) is simplified as

$$G(\vec{r},\vec{r}') = \frac{-2}{\pi\varepsilon_v}\int_0^{\infty} dk\, \left[\sum_{m=-\infty}^{+\infty} q_m(k)\frac{I_m(ka)}{K_m(ka)}K_m(k\rho_<)K_m(k\rho_>)\right]. \quad (6)$$

In figure 1, the location of the positive charge in the dipole is $Z = l/2$, while that of the negative charge is $Z = -l/2$. With Eq. (6), the total electric potential $V_{Z=l/2}$ at the location of the positive charge of the dipole, produced by all image charges associated with both the positive and negative charges in the dipole, is expressed as

$$V_{Z=l/2} = \frac{-2}{\pi}\int_0^\infty dk \left\{ \left[\sum_{m=-\infty}^{\infty} q_m(k) \frac{I_m(ka)}{K_m(ka)} [K_m(k\rho)]^2 \right] + \left[\sum_{m=-\infty}^{\infty} \left(-q_m(k)\right) \frac{I_m(ka)}{K_m(ka)} K_m(k\rho) K_m(k\rho + kl) \right] \right\}, \quad (7)$$

where the first square bracket term is the contribution from the image charges associated with the positive charge of the dipole and is obtained by letting both $\rho_<$ and $\rho_>$ equal ρ_+ (note $\rho_+ = \rho$) in Eq. (6). Note that for the first square bracket term, both the field point and the source point are at the location where the positive charge resides. The second bracket term in Eq. (7) is the contribution from the image charges associated with the negative charge and is obtained by letting $\rho_< = \rho_+ = \rho$ and $\rho_> = \rho_- = \rho + l$ in Eq. (6). Note that for the second square bracket term, the field point is at the location where the positive charge resides, and the source point is at the location where the negative charge resides. Because the second square bracket term in Eq. (7) is associated with the negative charge, there is a negative sign in front of $q_m(k)$. In the derivation of Eq. (7), $\varepsilon_v = 1$ is used. So, we have

$$E_1 = q\, V_{Z=l/2} = \frac{-2q}{\pi}\int_0^\infty dk \left[\sum_{m=-\infty}^{\infty} q_m(k) \frac{I_m(ka)}{K_m(ka)} [K_m(k\rho)]^2 \right] + \frac{2q}{\pi}\int_0^\infty dk \left[\sum_{m=-\infty}^{\infty} q_m(k) \frac{I_m(ka)}{K_m(ka)} K_m(k\rho) K_m(k\rho + kl) \right]. \quad (8)$$

Similarly,

$$\begin{aligned} E_2 &= -qV_{Z=-l/2} \\ &= \frac{2q}{\pi}\int_0^\infty dk \left[\sum_{m=-\infty}^{\infty} -q_m(k) \frac{I_m(ka)}{K_m(ka)} [K_m(k\rho + kl)]^2 \right] \\ &\quad + \frac{2q}{\pi}\int_0^\infty dk \left[\sum_{m=-\infty}^{\infty} q_m(k) \frac{I_m(ka)}{K_m(ka)} K_m(k\rho) K_m(k\rho + kl) \right]. \end{aligned} \quad (9)$$

The electrostatic interaction energy E_{dipole}^{static} is expressed as,

$$E_{dipole}^{static} = E_1 + E_2 = \frac{-2q}{\pi}\int_0^\infty dk \sum_{m=-\infty}^{\infty} q_m(k) \frac{I_m(ka)}{K_m(ka)} [K_m(k\rho) - K_m(k\rho + kl)]^2, \quad (10)$$

which properly vanishes $\sim(ql)^2$ when $ql \to 0$. From this result, the total final vdW energy between the instantaneous dipole and the cylinder can be evaluated as (the full derivation can be found in the Appendix),

$$E_{vdW} = -\frac{2}{\pi}\sum_{m=-\infty}^{\infty}\int_0^\infty dk \int_0^\infty du\, \alpha_1(iu)\, \xi_m(k,\rho)\, \Gamma_m(u,k) \left(\frac{D}{D+\bar{b}}\right)^2 \quad (11)$$

In Eq. (11), the damping function $\left(\frac{D}{D+\bar{b}}\right)^2$ is added to correct the spurious divergence as $D \to 0$. $\bar{b}$ is a cutoff parameter and will be discussed in the following paragraphs. The function $\xi_m(k,\rho)$ is defined as

$$\xi_m(k,\rho) = \frac{I_m(ka)}{K_m(ka)}[K_m'(k\rho)\ k]^2\ . \qquad (12)$$

In Eq. (11), $\Gamma_m(u,k)$ is defined as

$$\Gamma_m(u,k)\ = \frac{\varepsilon(iu)-1}{\varepsilon(iu)-h_m(k)}\ , \qquad (13)$$

and $\alpha_1(0)$, $\bar{b}$, ω_1, and ω_p will be defined in the next two paragraphs. Eq. (11), along with Eqs. (5), (12), and (13), are the working equations for our calculations. As will be shown in the Results and Discussion section, Eq. (11) varies as $D^{-4.5}$ around $D = 50$Å, and as D^0 when $D \to 0$.

A (n,m) CNT can be semiconducting or metallic, dependent on tube chirality. The armchair (n,n) CNTs are usually metallic and their longitudinal polarizabilities or dielectric constants are extremely large [49, 50] whereas the $(n,0)$ zigzag CNTs can be semiconducting or semimetallic. The semiconducting and metallic nanotubes have similar dielectric responses in the direction perpendicular to the tube axis, while their responses along the tube axis are very different [50]. In principle, our method can apply to any nanotube, whether metallic or semiconducting, as long as the dielectric function of the tube can be properly approximated. As a simplest model, the dielectric response of a metallic nanotube can be modeled as that of a free-electron gas. Since the nanotube considered in this work is semiconducting, we use the modified Penn model to express the dynamic dielectric function, $\varepsilon(iu)$, of the semiconducting cylinder [51,52]. It reads

$$\varepsilon(iu) = 1 + \frac{\omega_p^2}{u^2}\left[\frac{(1-\Delta^2)y}{P} - \frac{\omega_g^2 - \left(\omega_g^2+u^2\right)\Delta^2}{2u\sqrt{\omega_g^2+u^2}}\ln\frac{I_+}{I_-}\right] + \frac{2\omega_p^2\Delta}{u^2}\left\{\frac{\omega_g}{u}\left[\tan^{-1}\left(\frac{\omega_g P}{u}\right) - \tan^{-1}\left(\frac{\omega_g}{u}\right)\right] + \frac{1}{P} - 1\right\}. \qquad (14)$$

Here, $I_\pm = \left[(1+y^2)(1+u^2/\omega_g^2)\right]^{1/2} \pm uy/\omega_g$, $y = 1/\Delta$, and $P = (1+y^2)^{1/2}$. ω_g is the effective energy gap, which is defined below, and $\Delta = \omega_g/(4\varepsilon_F)$ with $\varepsilon_F = (3\pi^2\ n_{nanotube})^{2/3}/2$, with $n_{nanotube}$ defined in the second paragraph after Eq. (15). This model dielectric function has been used to study physical adsorption [51, 53, 54]. The effective energy gap ω_g is related to the static dielectric function $\varepsilon(0)$ via the Penn model [55],

$$\varepsilon(0) = 1 + \frac{2\omega_p^2}{3\omega_g^2}\left[(1+\Delta^2)^{1/2} - \Delta\right]. \qquad (15)$$

Since the accurate $\varepsilon(0)$ from a high-level *ab initio* calculation contains important hybridization, inhomogeneity, and exciton effects, which can be carried over to our model via the Penn model, the model dielectric function is expected to work well for semiconductors [54]. For a (10,0) semiconducting

CNT, the average static dielectric function is evaluated as $\varepsilon(0) = 12.91$ from the data in ref. [50, 56]. ω_g is determined to be 0.289 atomic unit by Eq. (15).

In the derivation of Eq. (11), the case of a cylinder with a large radius a is considered and an analogy to the flat-surface Zaremba-Kohn formula is also made (details see Appendix). This leads to Eq. (11) having features of the Zaremba-Kohn formula. However, Eq. (11) is a modification to a curved cylindrical surface. We call our model vdW-dZK (damped Zaremba-Kohn). Based on the estimated reference values (see Table 1), the cutoff parameter $\bar{b}$ is fitted by optimizing the mean errors (ME), root mean squared errors (RMSE), mean absolute errors (MAE), and mean absolute percentage errors (MAPE), and consequently chosen by an "eyeball estimation" to be 1.7 Bohr (0.899 Å) for the PBE functional and 4.5 Bohr (2.38 Å) for the SCAN functional. A larger $\bar{b}$ results in a damping factor that turns on the long-range dispersion only at larger D. Note that the cutoff parameter $\bar{b}$ is relatively large for SCAN, due to the capture of intermediate correlations by SCAN. This is consistent with our previous work on layered materials, where $\bar{b}$ was relatively larger for SCAN-vdW-dZK than PBE-vdW-dZK.

The diameter of a (n, m) nanotube can be found as $d = \frac{\sqrt{3}\, a_{C-C}}{\pi}\sqrt{m^2 + mn + n^2}$ [31], where a_{C-C} is the nearest C-C distance (1.42 Å) [31]. Accordingly, the radius $a = d/2$ of the (10,0) nanotube is 7.398 Bohr (3.915 Å). We treat NH_3 and NO_2 molecules interacting with a nanotube as a collection of renormalized atoms (see Ref. [45] for details). Each atom has its renormalized static polarizability $\alpha_1(0)$ [45,57]. For example, the renormalized static polarizability is 5.034 atomic units for N and 3.052 atomic units for H in the NH_3 molecule, while it is 7.988 atomic units for N and 5.824 atomic units for O in the NO_2 molecule. The dynamic polarizability of each renormalized atom is calculated as $\alpha_1(iu) = \alpha_1(0)\frac{\omega_1^2}{(\omega_1^2+u^2)}$ with $\omega_1 = \sqrt{4\pi\frac{n_{molecule}}{3}}$. where $n_{molecule}$is the average valence electron density within the molecule [44, 45]. Furthermore, $\omega_p = \sqrt{4\pi n_{nanotube}}$. The carbon nanotube can be formed by rolling up a graphene sheet. The average electron density of the carbon nanotube can be approximated as that of the graphene sheet and is $n_{nanotube} = \frac{8}{\left[\left(\frac{2.46}{0.529}\right)^2 \times \frac{\sqrt{3}}{2} \times 3.4\right]} = 0.126$ atomic unit [43, 44].

Although individual factors in the integrand of Eq. (11) are highly divergent as $k \to 0$, the integrand itself has only a weak $1/\ln k$ divergence as $k \to 0$, and decays like $e^{-2k(\rho-a)}$ as $k \to \infty$. In the evaluation of Eq. (11), the integral over u is performed first; followed by the integral over k and then the summation over m. It is found that for distances D ranging from 2.1 to 10.1 Bohr (1.11 Å to 5.34 Å), the results obtained from the k grid of (0.001, 40, 0.001) and the m range of (0, 20, 1) deviate from those from the k grid of (0.001, 46, 0.001) and the m range of (0, 40, 1) by less than 0.03%. Note that we adopted the notation $(x_{min}, x_{max}, x_{increment})$ to describe the computation grids where x_{min} is the starting point, x_{max} is the ending point, and $x_{increments}$ is the increment. Within the same distance range, the results from the k grid of (0.001, 40, 0.001) and the m range of (0, 20, 1) are the same as those from the k grid of (0.001, 20, 0.001) and the m range of (0, 20, 1). Furthermore, within the same distance range, when using a denser k grid, the results from the k grid of (0.0001, 40, 0.0001) and the m range of (0, 20, 1) are different from those from the k grid of (0.001, 40, 0.001) and the m range of (0, 20, 1) by less than 0.2%. The above tests are done for the u grid of (0.01, 30, 0.01). At the k grid of (0.001, 40,

0.001) and the m range of (0, 20, 1), when using the u grid of (0.001, 50, 0.001), the deviation is less than 0.07%. For computational efficiency, we use the k grid of (0.001, 40, 0.001), the m range of (0, 20, 1) and the u grid of (0.01, 30, 0.01) for the rest of the calculations. Since the equilibrium distances of the systems studied here are within this distance range, the results obtained here show acceptable convergence.

The form of the vdW-dZK Eq. (11) for a conducting cylindrical surface is very different from the expressions we obtained before for a flat metallic surface [43, 44] or a flat semiconducting layered material surface [46], although they all bear the same physics of the Zaremba-Kohn formula [42]. Only the dipolar effect is included in Eq. (11). High order terms, such as quadrupole terms, are very complicated and not included. Similar to the formula for a finite thickness semiconducting layered material surface slab, the multiple image effects are included in Eq. (11), however, through a complicated form with the modified Bessel functions. The parameter m can be regarded as an image index. However, the complicated form in Eq. (11) reflects the complexity of the shape and distribution of the images in the cylinder.

RESULTS AND DISCUSSION

The (10,0) CNT is shown in Fig. 2. It is modelled by making a supercell (enclosed by faint lines in Fig. 2) of eight layers of carbon along the tube axis so that 80 atoms are included in the cell. The size of the supercell is about $28 \times 30 \times 8$ Angstroms. The CNT is constructed with a nearest carbon-carbon distance of 1.42 Å, then one NH_3 molecule is placed near the tube wall. Two rotational geometries are considered, as shown in Figs. 2a and 2b denoted type I and type II. The setup for the CNT + NO_2 system is similar. Two geometries of CNT + NO_2 are also considered, type I and type II, as shown in Figs. 2c and 2d, respectively.

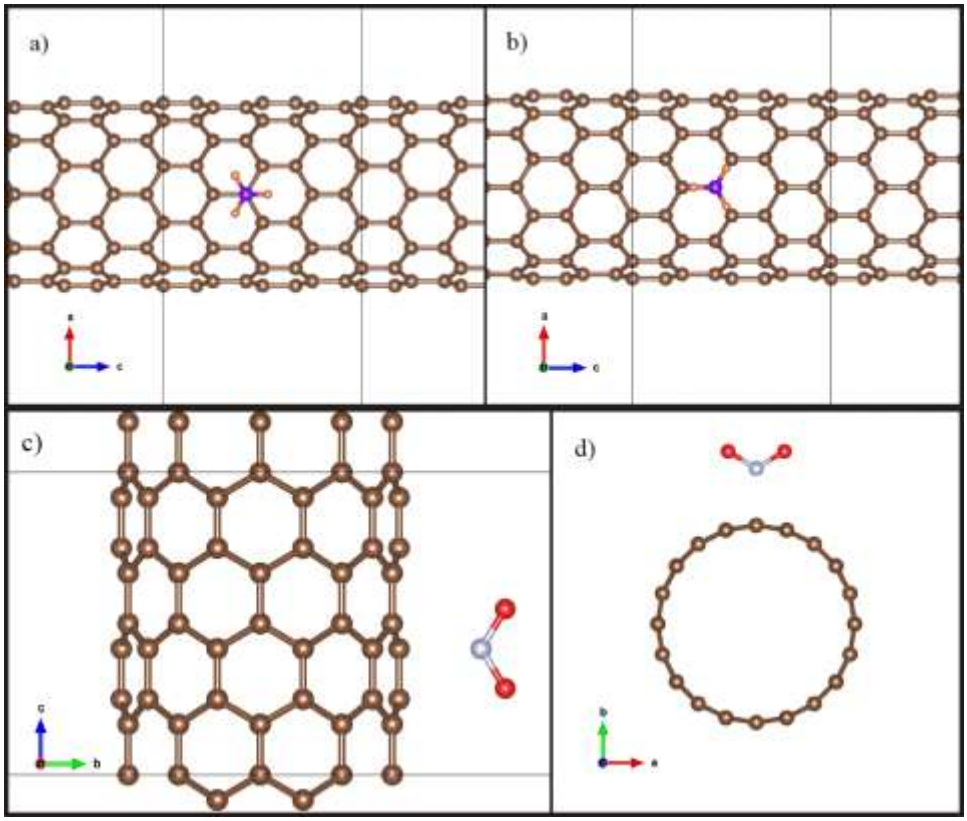

FIG. 2. (10,0) CNTs with adsorbed NH_3 or NO_2 molecules. a) Top view of the NH_3 molecule attached to the CNT in Type I geometry. b) In Type II geometry. c) Side view of the NO_2 molecule attached to the CNT when the plane of the NO_2 is parallel to the axis of the CNT (Type I). d) Side view of the NO_2 molecule attached to the CNT when the plane of the NO_2 is perpendicular to the axis of the CNT (Type II).

All DFT calculations are done in the Vienna Ab initio Software Package (VASP) [58] with projector augmented wave (PAW) pseudopotentials [59, 60]. The 1.42 Å carbon-carbon nearest-neighbor distance is a starting value and the nucleus of the N atom (or O atom) of the molecule is initially placed 3 Å straight above the nearest carbon atom of the tube wall, see Fig. 2. First, the molecule-tube structure is relaxed. Then, from the relaxed structure, the distance between molecule and tube is varied and the DFT binding energies at different distances are calculated so that the DFT curves of binding energy vs. distance are obtained. For the vdW energy calculations of the renormalized N atom (or O atom) in the molecule, the distance D is the distance between the nucleus of the N atom (or O atom) in the molecule and that of the nearest carbon atom. For the renormalized H atoms in the molecules, D is the distance between the nucleus of the H atom and the surface of a cylinder with the radius of the carbon nanotube. The energy cutoff is 580 eV. The k-point mesh is $1 \times 1 \times 3$. The structure optimization is conducted with all forces less than 0.01eV/Å. The binding energy is defined as the total energy of the molecule-nanotube structure after subtraction of the energy of the separated CNT and the energy of the separated molecule. Several Python scripts are written to compute the vdW energies using Eq. (11) for different distances, and the results are then combined with the DFT results to get the total binding energy curve, whose minimum is the equilibrium point, hence the equilibrium binding energy E_b and the equilibrium distance D_{eq}. The flow chart of the computational process is shown in Fig. 3. For comparison, the results from the SCAN+rVV10 and PBE+rVV10 calculations are also presented in Table I.

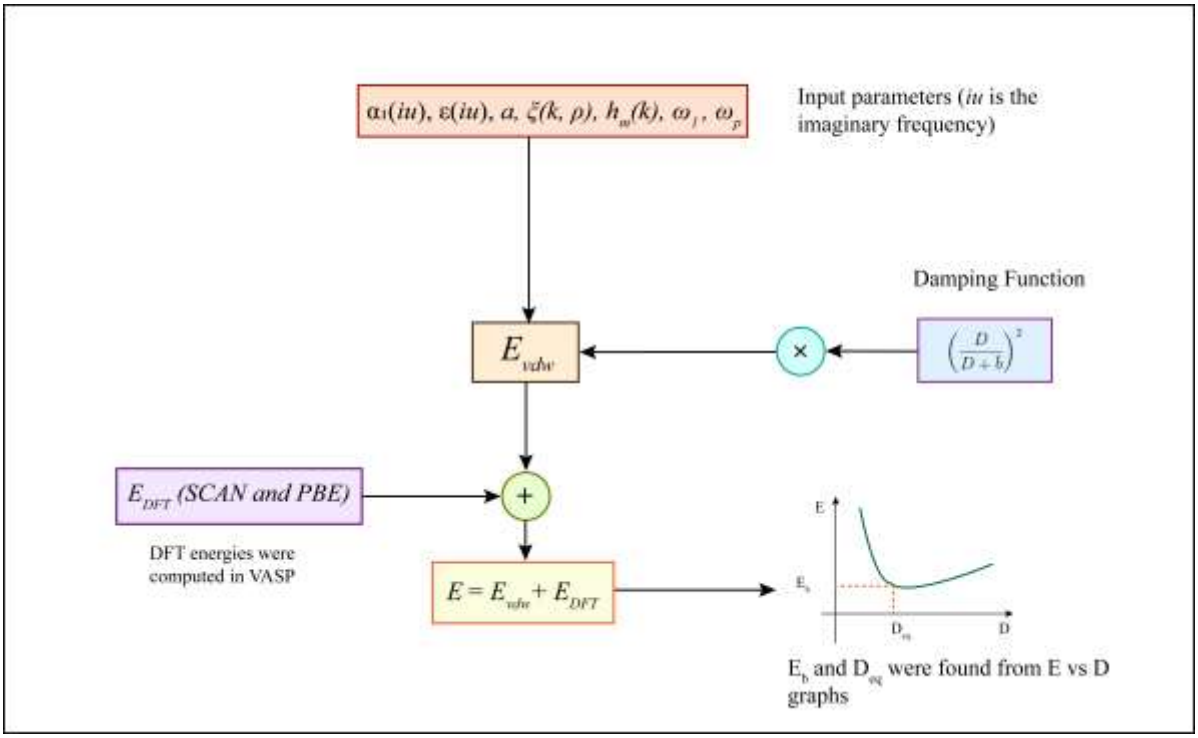

FIG. 3. Flow chart of the computational process for the vdW interaction energies, DFT energies, and total energies for the developed PBE-vdW-dZK and SCAN-vdW-dZK methods.

TABLE I. The binding energies E_b (meV) and equilibrium distances D_{eq} (Angstrom) calculated from different methods for NH_3 and NO_2 molecules adsorbed on a (10,0) single-wall carbon nanotube.

	Ref. (estimated here)	SCAN		SCAN+rVV10		SCAN-vdW-dZK		PBE		PBE+rVV10		PBE-vdW-dZK	
	E_b	E_b	D_{eq}	E_b	D_{eq}	E_b	D_{eq}	E_b	D_{eq}	E_b	D_{eq}	E_b	D_{eq}
Type I CNT + NH_3	-100	-43.3	3.38	-80.5	3.27	**-103.4**	**3.22**	-18.5	3.77	-70.8	3.44	**-114.2**	**3.26**
Type II CNT + NH_3	-100	-47.7	3.39	-84.2	3.31	**-107.8**	**3.22**	-18.4	3.77	-70.48	3.45	**-113.8**	**3.26**
Type I CNT + NO_2	-500	-354.3	2.70	-423.2	2.64	**-486.0**	**2.58**	-211.1	3.06	-309.3	2.80	**-441.3**	**2.59**
Type II CNT + NO_2	-500	-339.2	2.76	-402.7	2.69	**-462.4**	**2.62**	-207.7	3.16	-296.8	2.86	**-422.3**	**2.62**

As can be seen from Table I, PBE captures no long-range and very little intermediate-range vdW interaction and yields an unphysically weak binding energy (~ -18.5 meV for CNT + NH_3 and -210 meV for CNT + NO_2). Furthermore, it results in a relatively large equilibrium distance of about 3.77 Å for CNT + NH_3 and about 3.06 Å for CNT + NO_2. SCAN is designed to satisfy all 17 exact constraints that

a meta-GGA functional can satisfy and can capture intermediate range (on the length scale of about 3 Å) vdW interactions about right. Thus, SCAN gives a better description than does PBE. SCAN yields about half of the binding energies, compared with the reference, and shorter equilibrium distances than PBE does. Since it has been proven that SCAN is much more accurate than previous semilocal DFT methods, especially for geometrical and mechanical properties of materials, the equilibrium distances from SCAN should be closer to the real ones than those from PBE are. This is also consistent with the results we obtained in our layered material work [46].

As semilocal functionals, neither PBE nor SCAN include long-range vdW interactions. By adding the long-range vdW corrections (rVV10 or vdW-dZK) to PBE or SCAN, much better binding energies are achieved. This shows the significance of vdW energy in computing the total binding energy in the systems considered here. However, since the molecule-nanotube systems considered here are relatively large (>80 atoms), there is no high-level computational result in the literature, to the authors' best knowledge. The available binding energies E_b and equilibrium distance D_{eq} for NH_3 and NO_2 molecules adsorbed on carbon nanotubes from the literature are calculated with LDA, PBE+D, or vdW-DF functionals. For CNT+NH_3, Ref. [61] gives E_b = -0.15eV and D_{eq} = 2.99 Å with LDA. Ref. [62] gives E_b = -0.14eV and D_{eq} = 3.08 Å with LDA. Ref. [36] gives E_b = -0.18eV and D_{eq} = 2.90 Å with LDA. However, Ref. [63] gives E_b = -0.043eV and D_{eq} = 3.50 Å with vdW-DF. For CNT+NO_2, Refs. [36, 61, 64] show that the binding energy ranges from -0.34 to -0.79 eV, and the equilibrium distance ranges from 1.93 to 2.61 Å . However, Ref. [63] gives E_b = -0.26eV and D_{eq} = 3.20 Å with PBE+D. Based on these data, we estimate average values of binding energies for the two systems. The estimated values of binding energies are also listed in Table I. The estimated references listed here can only serve as a rough guideline. Nevertheless, the results shown in Table I give a clear trend, from which we can find some physically relevant clues.

For NH_3 adsorbed on the carbon nanotube, the two adsorption configurations (Types I and II) have very similar binding energies. The predicted values of the binding energies using SCAN, SCAN+rVV10, and SCAN-vdW-dZK are slightly smaller for Type I than for Type II, while the predicted values of the binding energies using PBE, PBE+rVV10 and PBE-vdW-dZK are slightly larger for Type I than for Type II. For NO_2 adsorbed on the nanotube, the predicted binding energies (about 200-500meV) are higher than the case of CNT+NH_3. It was reported [36] that CNTs respond more quickly and sensitively to NO_2 gas than to NH_3 gas. This is clearly illustrated by stronger binding energy from NO_2 than from NH_3. All methods in Table I predict that the binding energies from type I are slightly larger than those from type II for CNT+NO_2. However, the differences in binding energies between the two configurations for both CNT+NH_3 and CNT+NO_2 are very small, indicating similar binding stability between the two configurations [36]. Moreover, the values of the binding energies are relatively small ($\leq$ 500 meV) for both CNT+NH_3 and CNT+NO_2, indicating that the adsorption of the two molecules on nanotubes is physisorption.

With the combinations of the long-range vdW functional rVV10, both PBE and SCAN significantly improve in their descriptions for binding energies. However, PBE+rVV10 produces about 15% and 25% lower binding energies than SCAN+rVV10 does for CNT+NH_3 and CNT+NO_2, respectively. SCAN+rVV10 delivers a generally improved description for many systems. However,

SCAN+rVV10 has some serious issues, including the overestimated equilibrium mass density in liquid water [65], inaccurate structural and mechanical properties in PPTA [66], overestimated binding energies of thiophene molecule adsorbed on metal surfaces [45] and graphene adsorbed on transition metal dichalcogenide multilayer materials [46], and inconsistent errors of overbinding and underbinding in different 2D materials [67]. The drawback of SCAN+rVV10 may be due to its imperfect balance of interactions at the intermediate range. At present, although the results of SCAN+rVV10 seem very reasonable, it is hard to determine its accuracy, due to the shortage of accurate reference data. The same imperfect balance of interactions at the intermediate range also exists in PBE+rVV10. This leads to the limited accuracy of PBE+rVV10.

When combined with the developed vdW-dZK method, both PBE and SCAN improve in their descriptions of adsorption for CNT+NH_3 and CNT+NO_2 significantly. As can be seen in Table I, SCAN-vdW-dZK and PBE-vdW-dZK give approximately the same results for CNT+NH_3. For CNT+NO_2, although PBE-vdW-dZK gives about 10% lower binding energies than does SCAN-vdW-dZK, the results of binding energies from SCAN-vdW-dZK and PBE-vdW-dZK are the closest to each other. This also shows the consistency of our developed SCAN-vdW-dZK and PBE-vdW-dZK methods. Based on this consistency, it seems that the results from SCAN-vdW-dZK and PBE-vdW-dZK are closer to the real ones. There are still gaps between the results of SCAN-vdW-dZK and PBE-vdW-dZK and the estimated reference in table I. However, since the estimated references are averages of limited data from the literature, the references present just a rough guideline, not an accurate one.

Ambrosetti et al. [68] have shown nontrivial variations of power-laws of the vdW interactions in systems of atoms or small molecules and 2D thin metallic or finite-gap substrates with RPA-like and CDH (coupled dipolar Hamiltonian) treatments for substrate responses. They provided evidence to support the claim that the power laws of vdW interactions substantially deviate from the standard pairwise predictions. The power-law exponent $P(D)$ is defined as $P(D) = d(log|E_{vdw}|)/d\log D$, and is a decaying function of separation D. We also calculate the vdW interaction energy power laws from our vdW-dZK model for the CNT+NH_3 and CNT+NO_2 systems. Fig. 4 shows the vdW power-law exponent from our vdW-dZK model as a function of D. It shows that the vdW-dZK exponent is zero at small D. The behavior of the power law exponent at small distance (< 10 Å) is more influenced by the damping function. At distances D about 20 Å, the exponent is about -4.0 and at distances D about 50 Å, the exponent is about -4.5, clearly keeping away from the pairwise limit -5. This feature is very similar to the one calculated by Ambrosetti et al., see the second curve in the upper figure of FIG. 2 in Ref. [68], where the lattice constant of the carbon atom chain is 1.4 Å, very close to that of the carbon nanotube. In Ref. [68], the results are obtained from RPA and RG (renormalization group) approaches. The similarity between our results and that of Ref. [68] provides support to our methods. The finite (~3.9Å) radius of the carbon nanotube and the damping factor are also at play in our results.

(a)

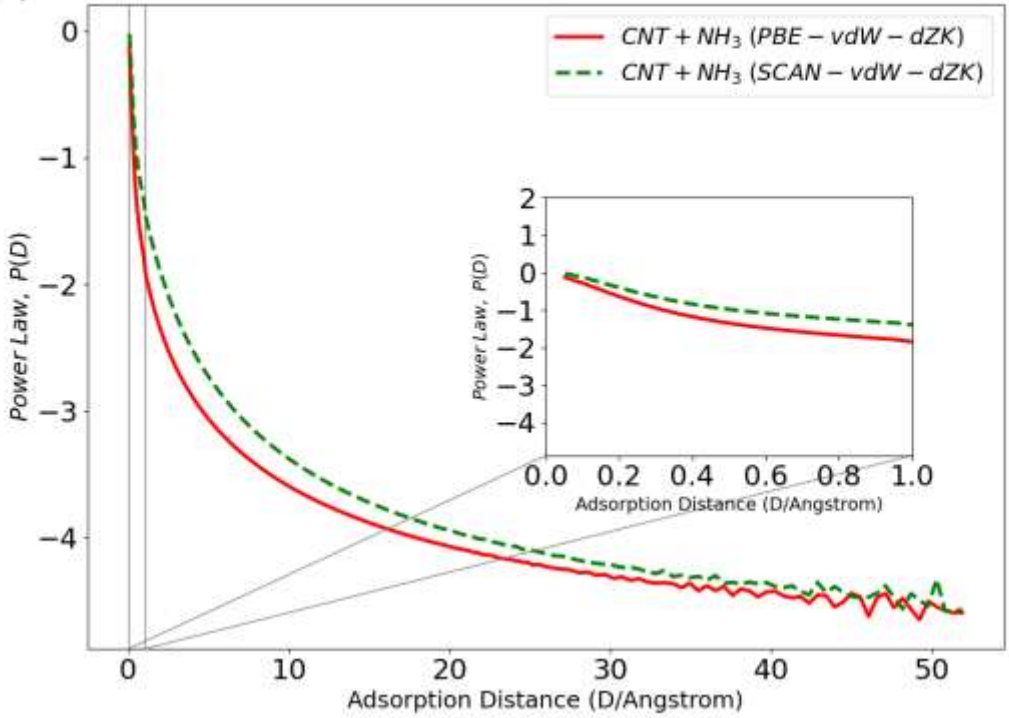
CNT + NH3 (PBE − vdW − dZK)
CNT + NH3 (SCAN − vdW − dZK)
Power Law, P(D)
Adsorption Distance (D/Angstrom)
0
−1
−2
−3
−4
0
10
20
30
40
50
2
1
0
−1
−2
−3
−4
0.0
0.2
0.4
0.6
0.8
1.0

(b)

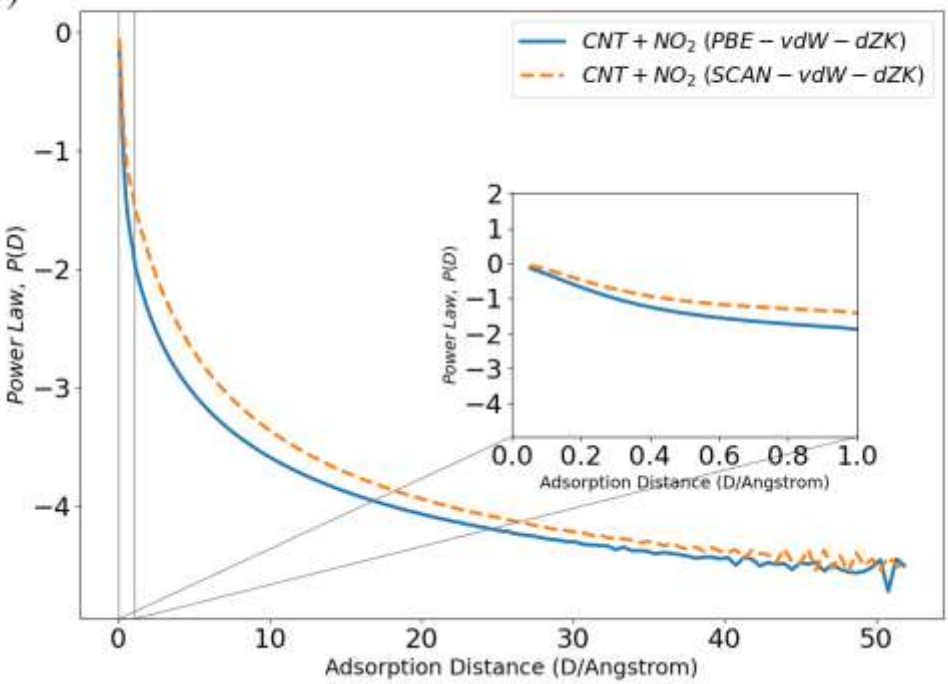
CNT + NO2 (PBE − vdW − dZK)
CNT + NO2 (SCAN − vdW − dZK)
Power Law, P(D)
Adsorption Distance (D/Angstrom)
0
−1
−2
−3
−4
0
10
20
30
40
50
2
1
0
−1
−2
−3
−4
0.0
0.2
0.4
0.6
0.8
1.0

FIG. 4. vdW interaction energy power law exponents from the vdW-dZK model for (a) NH_3 and (b) NO_2 molecules adsorbed on CNT as a function of adsorption distance D.

SUMMARY

We have developed a vdW interaction model for molecules adsorbed on curved cylindrical conducting surfaces, and have combined this model with the semilocal density functionals PBE and SCAN. The resulting PBE-vdW-dZK and SCAN-vdW-dZK are applied to NH_3 and NO_2 adsorbed on carbon nanotubes. The results from PBE-vdW-dZK and SCAN-vdW-dZK are also compared with those from vdW nonlocal functionals, such as SCAN+rVV10 and PBE+rVV10. The PBE functional captures almost no vdW interaction and underestimates the binding energies for the two systems. Even without the inclusion of long-range vdW interactions, SCAN can capture intermediate vdW interactions and gives much improved binding energies. When combined with the vdW-dZK model and vdW functional rVV10, both PBE and SCAN improve their descriptions for these systems in which vdW interaction is important. Generally speaking, the binding energies from PBE+rVV10, SCAN+rVV10, PBE-vdW-dZK, and SCAN-vdW-dZK are roughly the same, about 70-115meV for CNT+NH_3 and 300-490meV for CNT+NO_2, respectively. The results from PBE-vdW-dZK and SCAN-vdW-dZK are closer to each other than are those of PBE+rVV10 and SCAN+rVV10. For CNT+NH_3, PBE-vdW-dZK and SCAN-vdW-dZK give binding energies of about 103-114 meV. For CNT+NO_2, PBE-vdW-dZK and SCAN-vdW-dZK give binding energies of about 422-490 meV. Comparatively, for CNT+NH_3, PBE+rVV10 and SCAN+rVV10 give binding energies of about 70-80meV, while for CNT+NO_2, they give about 300-420meV. The relatively closer results from PBE-vdW-dZK and SCAN-vdW-dZK indicate the consistency of our developed vdW-dZK model for curved surfaces. Due to the relatively large systems (>80 atoms) considered here, there is no high-level computational result. The available reference data from the literature can just serve as a rough guideline for the binding energies of the systems, and more reliable reference values would yield a more reliable damping factor $\bar{b}$ in Eq. (11). However, our vdW-dZK combined with PBE and SCAN gives results closer to this guideline than other methods considered here. It seems that the results from PBE-vdW-dZK and SCAN-vdW-dZK could be more realistic. All methods, including PBE, SCAN, PBE+rVV10, SCAN+rVV10, PBE-vdW-dZK, and SCAN-vdW-dZK, give approximately the same binding energies for the two adsorption configurations (types I and II) for the two systems. This may imply that the two-adsorption sites have approximately the same adsorption stability.

The exponent of the vdW interaction power law from our vdW-dZK model for CNT+NH_3 and CNT+NO_2 systems is about 0 at short distance, largely due to the damping factor. At distances D about 20-50 Å, the exponent is about -4.0 ~ -4.5, and not the pairwise limit -5. This feature is very similar to the one calculated by RPA and RG (renormalization group) approaches. This similarity provides further support to our methods.

ACKNOWLEDGEMENTS

S.T.U.R.C. and H.T. acknowledge support from the DOE Office of Science, Basic Energy Sciences (BES), under Grant No. DE-SC0018194. J.P.P. and S.T.U.R.C. were supported by NSF Grant No. DMR-

1939528. Computational support was provided by NERSC, EFRC, as well as by HPC of Temple University. The authors thank the referee for substantive suggestions that have improved this work.

APPENDIX

In this appendix, we present the derivation of Eq. (11). The starting point to derive Eq. (11) is the general form of the electric potential produced by the image charge residing inside the cylindrical medium. It is given by Eq. (6). The electrostatic interaction energy E_{dipole}^{static}, between the dipole and the cylinder, is given by Eq. (10).

With the expression for $q_m(k)$ in Eq. (4) (with $\varepsilon_v = 1$) and the condition $l \ll \rho$, Eq. (10) can be written as

$$E_{dipole}^{static} = \frac{-2q^2l^2}{\pi}\sum_{m=-\infty}^{\infty}\int_0^{\infty} dk\,\frac{\varepsilon-1}{\varepsilon-h_m(k)}\frac{I_m(ka)}{K_m(ka)}[K_m'(k\rho)k]^2$$
$$= \frac{-2q^2l^2}{\pi}\sum_{m=-\infty}^{\infty}\int_0^{\infty} dk\,\xi_m(k,\rho)\frac{\varepsilon-1}{\varepsilon-h_m(k)}\ , \qquad \text{(A1)}$$

where the function $\xi_m(k,\rho)$ is defined in Eq. (12).

When the radius of the cylinder becomes large, $a \to \infty$, the cylinder becomes a flat surface with infinite thickness. The problem becomes one in which an instantaneous dipole interacts with a flat surface of a solid. For this situation, when the distance D between the dipole and the surface is large, the vdW interaction energy is given by the Zaremba-Kohn formula as [42],

$$E^{ZK} = -\frac{1}{4\pi D^3}\int_0^{\infty} du\,\alpha_1(iu)\frac{\varepsilon(iu)-1}{\varepsilon(iu)+1} \qquad \text{(A2)}$$

where $\varepsilon(iu)$ is the dynamic dielectric constant of the surface, and $\alpha_1(iu)$ is the dynamic dipolar polarizability of the adsorbate. The time average of Eq. (A1) will lead to Eq. (A2) at large a and large D. With the asymptotic expressions for the modified Bessel functions [69], i.e., when $x \to \infty, I_m(x) \to e^x/\sqrt{2\pi x}$ and $K_m(x) \to e^{-x}\sqrt{\pi/(2x)}$, it can be shown that $h_m(k) \to -1$ as $a \to \infty$. Besides, we have

$$\lim_{a\to\infty}\frac{I_m(ka)}{K_m(ka)} \to \frac{e^{2ka}}{\pi}\ , \qquad \text{(A3)}$$

$$\lim_{a\to\infty}[K_m'(k\rho)]^2 \to \frac{\pi}{2k\rho}e^{-2k\rho} = \frac{\pi}{2k(D+a)}e^{-2k(D+a)}\ . \qquad \text{(A4)}$$

When $a \to \infty$ and $D \to \infty$, Eq. (A1) becomes

$$E_{dipole}^{static} \sim \frac{-2q^2l^2}{\pi}\frac{1}{8D^3}\frac{\varepsilon-1}{\varepsilon+1} = -\frac{q^2l^2}{4\pi D^3}\frac{\varepsilon-1}{\varepsilon+1}\,, \tag{A5}$$

taking a form similar to that of Eq. (A2). The time average of Eq. (A5) can be written as

$$\langle E_{dipole}^{static}\rangle_t \sim \frac{-2\langle q^2l^2\rangle_t}{\pi}\frac{1}{8D^3}\frac{\varepsilon-1}{\varepsilon+1} = -\frac{1}{4\pi D^3}\langle q^2l^2\rangle_t\frac{\varepsilon-1}{\varepsilon+1}\,, \tag{A6}$$

where the symbol $\langle X\rangle_t$ represents the time average of quantity $X(t)$. Since Eq. (A6) is equivalent to Eq. (A2), this means that $\langle q^2l^2\rangle_t\frac{\varepsilon-1}{\varepsilon+1}$ is equivalent to $\int_0^\infty du\,\alpha_1(iu)\frac{\varepsilon(iu)-1}{\varepsilon(iu)+1}$. We generalize this equivalence to a finite a and D, and write the time average of Eq. (A1) as

$$E_{vdW} = \langle E_{dipole}^{static}\rangle_t = -\frac{2}{\pi}\sum_{m=-\infty}^{\infty}\int_0^\infty dk\int_0^\infty du\,\alpha_1(iu)\,\xi_m(k,\rho)\,\Gamma_m(u,k) \tag{A7}$$

where $\alpha_1(iu)$ is defined after Eq. (13). Note that although ε in Eq. (A1) is time-independent under the electrostatic limit, it should be understood as frequency-dependent, as shown in Eq. (A7). The frequency dependent dielectric function is defined in the main text.

RFERENCES

[1] J. D. van der Waals, Doctoral Dissertation, Over de continuiteit van den gas-en vloeistoftoestand (On the Continuity of the Gaseous and Liquid States), Universiteit Leiden, Netherlands. 1873.

[2] V. A. Parsegian, Van der Waals Forces: A Handbook for Biologists, Chemists, Engineers, and Physicists. *(Cambridge University Press, 2005).*

[3] Reviews in Computational Chemistry. K. B. Lipkowitz, T. R. Cundari, *(Volume **26**. John Wiley & Sons. 2008)*

[4] M. J. Gillan, D. Alfè, and A. Michaelides, The Journal of Chemical Physics **144**, 130901 (2016).

[5] J. Hermann, R. A. DiStasio Jr., and A. Tkatchenko (2017). *Chemical Reviews*, *117*(6), 4714-4758.

[6] J. Tao, J. P. Perdew, and A. Ruzsinszky, Phys. Rev. B 81, 233102 (2010).

[7] R. A. DiStasio, Jr.; O. A. von Lilienfeld, A. Tkatchenko, Proc. Natl. Acad. Sci. U. S. A. 2012, 109, 14791−14795.

[8] K. Autumn, Y. A. Liang, S. T. Hsieh, W. Zesch, W. P. Chan, T. W. Kenny, R. Fearing, R. J. Full, Nature 2000, 405, 681−685.

[9] K. Autumn, M. Sitti, Y. A. Liang, A.M. Peattie, W. R. Hansen, S. Sponberg, T. W. Kenny, R. Fearing, J. N. Israelachvili, R. J. Full. Proc. Natl. Acad. Sci. U. S. A. 2002, 99, 12252−12256.

[10] B. Rozitis, E. MacLennan, J. P. Emery, (29075) 1950 DA. Nature 2014, 512, 174−176.

[11] D. J. Scheeres, C. M. Hartzell, P. Sá nchez, M. Swift. Icarus 2010, 210, 968−984.

[12] O. Gunnarsson and B. I. Lundqvist, Phys. Rev. B **13**, 4274 (1976).

[13] D. C. Langreth, and J. P. Perdew, Phys. Rev. B **15**, 2884 (1977).

[14] D. Pines, and D. Bohm, Phys. Rev. **85**, 338 (1952).

[15] D. Bohm, and D. Pines, Phys. Rev. **92**, 609 (1953).

[16] M. Dion, H. Rydberg, E. Schröder, D. C. Langreth, and B. I. Lundqvist, Phys. Rev. Lett. **92**, 246401 (2004).

[17] K. Lee, E. D. Murray, L. Kong, B. I. Lundqvist, and D. C. Langreth, Phys. Rev. B **82**, 081101 (2010).

[18] V. R. Cooper, Phys. Rev. B **81**,161104 (2010).

[19] J. Klimeš, D.R. Bowler, and A. Michaelides, J. Phys. Condens. Matter **22**, 022201 (2010).

[20] J. Klimeš, D. R. Bowler, and A. Michaelides, Phys. Rev. B **83**, 195131 (2011).

[21] I. Hamada, Phys. Rev. B **89**, 121103 (2014).

[22] K. Berland, and P. Hyldgaard, Phys. Rev. B **89**, 035412 (2014).

[23] O. A. Vydrov and T. Van Voorhis, J. Chem. Phys. **133**, 244103 (2010).

[24] R. Sabatini, T. Gorni, and S. de Gironcoli, Phys. Rev. B **87**, 041108 (2013).

[25] S. Grimme, J. Comput. Chem. 27, 1787–1799 (2006).

[26] S. Grimme, J. Antony, S. Ehrlich, and H. Krieg, J. Chem. Phys. **132**, 154104 (2010).

[27] A. Tkatchenko and M. Scheffler, Phys. Rev. Lett. **102**, 073005 (2009).

[28] A. Tkatchenko, R. A. DiStasio Jr., R. Car, and M. Scheffler, Phys. Rev. Lett. **108**, 236402 (2012).

[29] W. Liu, F. Ma, M. Willenbocke, C. Bronner, M. Schulze, S. Soubatch, F.S. Tautz, P. Tegeder, and A. Tkatchenko, Phys. Rev. Lett. **115**, 036104 (2015).

[30] S. Iijima, Nature London 354, 56 (1991).

[31] M. S. Dresselhaus, G. Dresselhaus, and P. C. Eklund, Science of Fullerenes and Carbon Nanotubes Academic, New York, 1996.

[32] S. J. Tans, M.H. Devoret, H. Dai, A. Thess, R.E. Smalley, L. Georliga, C. Dekker, Nature 386 (1997).

[33] R. H. Baughman, A. A. Zakhidov, W. A. de Heer, Science 297 (2002).

[34] S. J. Tans, A.R. Verschueren, C. Dekker, Nature 393 (1998).

[35] J. Kong, N. R. Franklin, C. Chou, M. G. Chaplin, S. Peng, K. Cho, and H. Dai, Science 287, 622 (2000).

[36] Chang, H., Lee, J. D., Lee, S. M., & Lee, Y. H. (2001). Applied Physics Letters, *79*(23), 3863-3865.

[37] W. Kohn and L. J. Sham, Phys. Rev. 140, A1133 (1965).

[38] J. P. Perdew, K. Burke, and M. Ernzerhof, Phys. Rev. Lett. **77**, 3865 (1996).

[39] J. Sun, A. Ruzsinszky, and J. P. Perdew, Phys. Rev. Lett. **115**, 036402 (2015).

[40] T. Emig, R. L. Jaffe, M. Kardar, and A. Scardicchio, Phys. Rev. Lett. 96(8), 080403 (2006).

[41] R. F. Rajter, R. Podgornik, V. A. Parsegian, R. H. French and W. Y. Ching, Phys. Rev. B 76(4) 045417 (2007).

[42] E. Zaremba and W. Kohn, Phys. Rev. B13, 2270 (1976).

[43] J. Tao, H. Tang, A. Patra, P. Bhattarai, J. P. Perdew, Phys. Rev. B **97**, 165403 (2018).

[44] H. Tang, J. Tao, A. Ruzsinszky, and J. P. Perdew, J. Phys. Chem. C, 123(22), 13748–13757 (2019).

[45] S. Adhikari, H. Tang, B. Neupane, A. Ruzsinszky, and G. I. Csonka, (2020). *Physical Review Materials*, *4*(2), 025005.

[46] H. Tang, S. T. U. R. Chowdhury, J. Tao, and J. P. Perdew (2020). Phys. Rev. B, *101*(19), 195426.

[47] J. A. Hernandes, and A. K. T. Assis (2005). Journal of electrostatics, 63(12), 1115-1131.

[48] S. T. Cui (2006). Molecular Physics, 104:19, 2993-3001.

[49] L. X. Benedict, S. G. Louie, M. L. Cohen, Phys. Rev. B 52, 8541-8549 (1995).

[50] B. Kozinsky, N. Marzari, Phys. Rev. Lett. 96, 166801 (2006).

[51] J. Tao, A. M. Rappe, Phys. Rev. Lett. **112**, 106101 (2014).

[52] R. A. Breckenridge, R. W. Shaw Jr., and A. Sher, Phys. Rev. B **10**, 2483-2489 (1974).

[53] G. Vidali and M. W. Cole, Surf. Sci. **107**, L374 (1981).

[54] F. Zheng, J. Tao, and A. M. Rappe, Phys. Rev. B. **95**, 035203 (2017).

[55] D. R. Penn, Phys. Rev. **128**, 2093 (1962).

[56] W. Lu, D. Wang and L. Chen, Nano Lett. *7*(9) 2729-2733 (2007).

[57] NIST Computational Chemistry Comparison and Benchmark Database. NIST Standard Reference Database Number 101, Release 20, August 2019, Editor: Russell D. Johnson III. http://cccbdb.nist.gov/

[58] G. Kresse, J. Furthmüller, Phys. Rev. B **54**, 11169 (1996).

[59] P. E. Blöchl, Phys. Rev. B **50**, 17953 (1994).

[60] G. Kresse, D. Joubert, Phys. Rev. B **59**, 1758 (1999).

[61] J. Zhao, A. Buldum, J. Han and J. P. Lu, Nanotechnology 13 (2002) 195–200.

[62] L. Bai, Z. Zhou. Carbon 45 (2007) 2105–2110.

[63] Y. Lia, M. Hodak, W. Lu, J. Bernholc. Carbon Volume 101 (2016), 177-183.

[64] S. Peng, K. Cho, P. Qi, H. Dai. Chemical Physics Letters 387 (2004) 271–276.

[65] J. Wiktor, F. Ambrosio, and A. Pasquarello, J. Chem. Phys. 147, 216101 (2017).

[66] J. Yu, G. Fiorin, H. Peng, M. L. Klein, and J. P. Perdew, *Physical Review Materials*, 4, 055601 (2020)

[67] M. Kim, W. J. Kim, T. Gould, E. K. Lee, S. Lebègue, and H. Kim, J. Am. Chem. Soc. 142, 2346 (2020).

[68] A. Ambrosetti, P. L. Silvestrelli, and A. Tkatchenko, Phys. Rev. B **95**, 235417 (2017).

[69] G.B. Arfken, H.J. Weber, and F.E. Harris, *Mathematical Methods for Physicists (Seventh Edition)*. Academic Press, 2013.